Supplementary Information

Iron single-atom catalysts created in constrained space with in-situ-formed carbon layers for efficient Fenton reaction

WANG Yang,[a,b] FAN Cun-Feng,[a,b] LIU Yang,[a,b] ZHENG Xiao-Qin,[a,b] LIU Xuan-Yi,[a,b] ZHANG Kai,[a,b] KOU Jiahui, *,[a,c] HUANG Hengming *,[a,c] and SUN Lin-Bing *,[a,b]

[a] State Key Laboratory of Materials-Oriented Chemical Engineering, 30 South Puzhu Road, Nanjing 211816, China. [b] College of Chemical Engineering, Nanjing Tech University, 30 South Puzhu Road, Nanjing 211816, China. [c] College of Materials Science and Engineering, Nanjing Tech University, 30 South Puzhu Road, Nanjing 211816, China.

Experimental details

Chemicals

All chemicals were used as received without further purification. Tetraethyl orthosilicate (TEOS) and $Fe(NO_3)_2 \cdot 6H_2O$ were purchased from Sinopharm Chemical Reagent Fe. Pluronic P123 ($EO_{20}PO_{70}EO_{20}$, Mn= ~ 5800) and hydrochloric acid (HCl, 37%) were purchased from Sigma Aldrich Ltd. Potassium hydroxide and potassium chloride were purchased from Aladdin Ltd. Deionized water was used throughout this study.

Materials synthesis

Synthesis of SBA-15. In a typical process, Pluronic P123 (2.0 g) was dissolved into the aqueous HCl solution (1.60 M, 75.0 g). Tetraethylorthosilicate (TEOS, 4.25 g) was added and stirred at 40 °C for 24 h, followed by the hydrothermal treatment at 100 °C for 24 h. After filtration and then drying under ambient conditions, the template-occupied SBA-15 (denoted as TLS) was recovered. After calcination in flowing air at 550 °C for 3 h, the template P123 was removed to get the template-free SBA-15 (denoted as TRS).

Synthesis of C-TLS. The support TLS was subjected to heat treatment in an Ar gas stream (200 $mL \cdot min^{-1}$) at a rate of 2 $°C \cdot min^{-1}$ from room temperature to 650 °C, yielding a carbonized sample named as C-TLS.

Materials characterization

X-ray diffraction **(**XRD) patterns were recorded on a Bruker D8 Avance diffractometer operated at 40 kV and 40 mA using a Cu Kα radiation (λ=0.15406 nm) at a step width of $2° \cdot min^{-1}$. The N_2 adsorption-desorption isotherms at 77 K were measured on a BELSORP-MAX analyzer. All of the samples were degassed at 393 K for 6 h. The pore size distribution was calculated from the Barrett-Joyner-Halenda (BJH) method according to the adsorption branch. Fourier transform infrared (FTIR) spectra were tested with a Nicolet Nexus 470 spectrometer at the spectra resolution of 2 cm^{-1}. Thermogravimetric (TG) analyses and their derivatives (DTG) were carried out on a thermobalance (STA-499C, NETZSCH). About 5 mg of sample was heated from room temperature to 800 °C in a flow of air (20 $mL \cdot min^{-1}$). X-ray photoelectron spectroscopy (XPS) analysis was performed using an ESCALAB-220I-XL (Thermo-Electron,

VG Company) device equipped with an Al Kα X-ray source (hv = 1486.6 eV) at 10 kV and 35 mA, and the binding energies were referred to C 1s at 284.8 eV. The morphology of the materials was identified by transmission electron microscopy (TEM, JEOL 2100F) operated at an accelerating voltage of 200 kV and aberration-corrected high-angle annular dark-field scanning transmission electron microscopy (HAADF-STEM, Titan Cubed Themis G2300). The X-ray absorption near edge structure (XANES) of Fe K-edge were performed at the BL11B beamline of Shanghai Synchrotron Radiation Facility (SSRF). The samples were ground and daubed uniformly on the unique double-sided carbon adhesive tape, the data were collected in fluorescence mode and the curves are normalized. The EXAFS spectroscopy measured with FLY (fluorescence yield) mode was numerically fitted by the real space multiple scattering program of FEFF9. Note: S_0^2 is the amplitude reduction factor, according to the experimental EXAFS fitted with of Fe foil reference by fixing CN as the known crystallographic value. ARTEMIS evaluates a variety of statistical parameters relevant to the evaluation of the fit. For example, E_0 is rarely more than 10 eV or less than -10 eV, that S_0^2 and σ^2 should never be negative. σ^2 value in the range between 0.001 and 0.01 will not be got a penalty. ARTEMIS software thinks any fit which *R*-factor has 2% or less misfit between data and theory is not assessed a penalty. The errors were automatically generated by the Athena and Artemis software.

DFT calculations

All quantum chemistry calculations were carried out using the ORCA software package[1, 2] with models of single-atom Fe anchored to graphene flake where the edges were capped by H atoms. For all structure optimization, the B97-3c[3] composite DFT method which is based on the B97 GGA including the D3(BJ) dispersion correction[4] with three-body contribution, a short-range bond length correction, and a modified, stripped-down triple-ζ basis termed def2-mTZVP. The resultant structures were verified as energy minima (all positive frequencies) and the free energy correction was carried out based on the vibrational frequency calculations performed at the same level. The transition states for O–O bond cleavage were confirmed by NEB-TS method in ORCA[5]. In order to simulate the solvent environment, an implicit solvation model of the Solvation Model based on Density (SMD)[6] is introduced for all models.

Table S1. Physicochemical properties of TRS, C-TLS, Fe_1@C-TLS and Fe@TRS

Sample	S_{BET} ($m^2 \cdot g^{-1}$)	V_p ($cm^3 \cdot g^{-1}$)	D_p (nm)	a_0 (nm)	Fe content (wt%) [a]
TRS	991	1.07	7.5	10.85	/
C-TLS	837	0.95	4.6	11.10	/
Fe_1@C-TLS	698	0.81	4.6	11.10	1.85
Fe@TRS	775	0.80	7.1	10.85	1.87

[a] The metal contents were determined by ICP-AES.

Table S2. EXAFS fitting parameters at the Fe K-edge for different samples (S_0^2 = 0.81)

Sample	Shell	CN	*R* (Å)	σ^2 (Å^2)	ΔE_0 (eV)	R factor
Fe foil	Fe-Fe	8	2.43±0.00	0.00125	5.30	0.0013
Fe_2O_3	Fe-O	6	1.95±0.00	0.00171	-6.56	0.0035
Fe_1@C-TLS	Fe-C	2.92±0.05	1.77±0.05	0.00609	-0.43	0.0142
Fe@TRS	Fe-O	4.50±1.57	1.81±0.02	0.01128	0.14	0.0151
	Fe-Fe	2.28±0.66	3.02±0.03	0.01863	1.26	

Table S3. Comparison of the catalytic activity of Fenton-like catalysts

Catalyst	Pollutant	Reaction conditions				Efficiency	k* (min^{-1})	Ref.
		[Catalyst] (g/L)	[Pollutant] (mg/L)	pH	[H_2O_2] (mmol/L)			
3%CNTs/Fh	Bisphenol A	1.0	30	3.0	10	96% in 30 min	0.008	[7]
30%HTC/Fh	Bisphenol A	1.0	30	3.0	10	100% in 20 min	0.016	[8]
SA-Cr/PN-g-C_3N_4	Bisphenol A	0.2	10	7.0	163	99% in 70 min	0.096	[9]
$CuFe_2O_4$	Sulfanilamide	0.1	0.55	6.5	15	82% in 5 h	0.006	[10]
CUS-MIL100 (Fe)	Sulfamethazin	0.5	20	4.0	6	100% in 60 min	0.009	[11]
CuCN	Tetracycline	0.5	20	7.0	80	94% in 60 min	0.008	[12]
45FePOM/CNNS	Tetracycline	1.0	20	4.5	10	97% in 18 min	0.015	[13]
SOH-600	Tetracycline	0.1	74	3.0	3	81% in 60 min	0.0023	[14]
Fe_1-N_v/CN	Ciprofloxacin	0.5	10	7.0	2.5	100% in 60 min	0.048	[15]
CuNiFeLa-LDHs	Ciprofloxacin	0.25	10	7.0	5	100% in 240 min	0.013	[16]
Fe-Pd@C	Phenol	0.5	47	5.0	10	100% in 10 min	0.040	[17]
MIL-88B-Fe	Phenol	0.1	50	4.0	15	99% in 30 min	0.008	[18]
1.0SAFe-SBA-15	Phenol	0.1	20	3.0	1	99% in 120 min	0.024	[19]
Fe_1@C-TLS	Phenol	0.1	20	3.0	1	99.7% in 40 min	0.102	This work

Table S4. Comparison of substrate residual amounts for Fenton-like catalysts at pH=5

Catalyst	pH	C/C_0	Ref.
Fe_1/O-graphene	5	70%	20
Fe_1/B-graphene	5	15%	20
FeS@NBCBM	5	15%	21
3%CNTs/Fh	5	10%	7
CUS-MIL-100(Fe)	5	20%	11
Fe_1@C-TLS	5	10%	This work

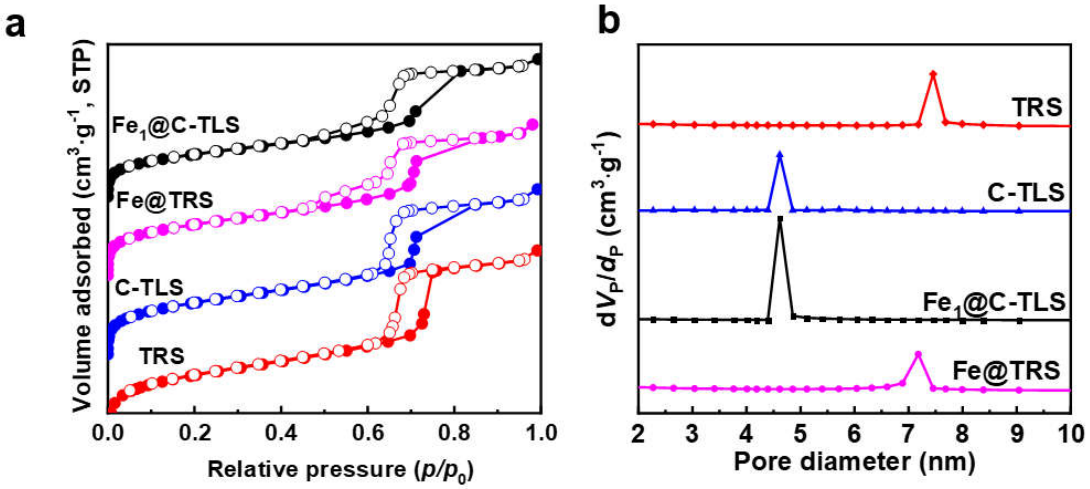

Fig. S1. (a) N_2 adsorption-desorption isotherms and (b) pore size distributions of TRS, Fe@TRS, C-TLS and Fe_1@TLS samples. Curves are plotted offset for clarity.

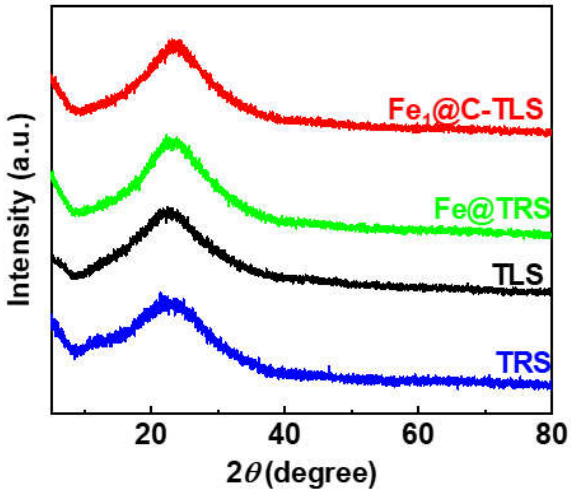

Fig. S2. XRD patterns of TRS, Fe@TRS, C-TLS and Fe_1@C-TLS samples.

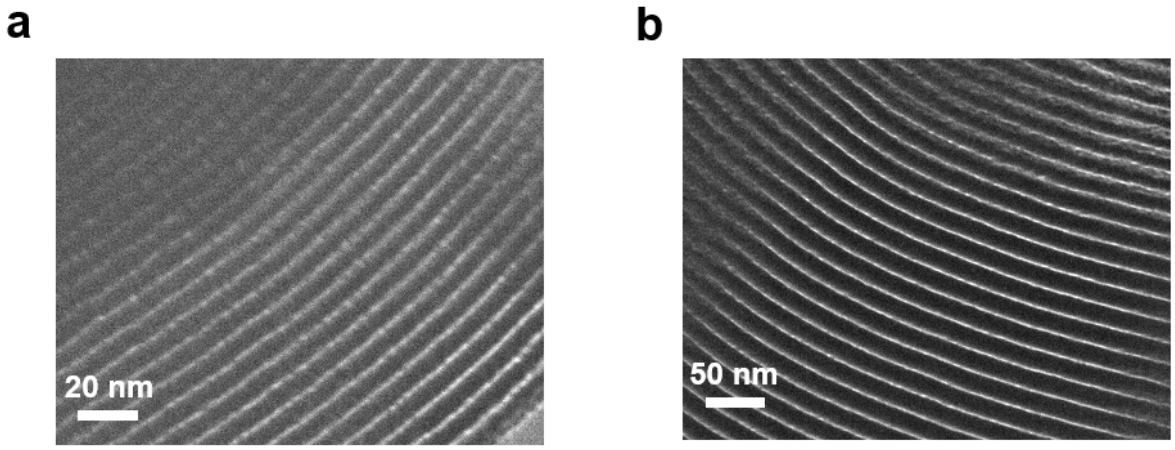

Fig. S3. TEM images of Fe_1@C-TLS.

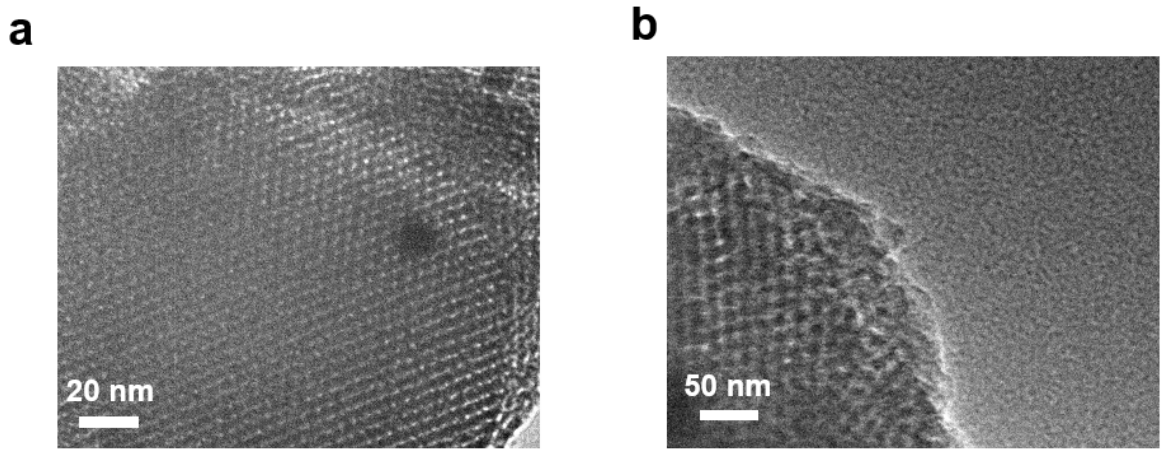

Fig. S4. TEM images of Fe@TRS.

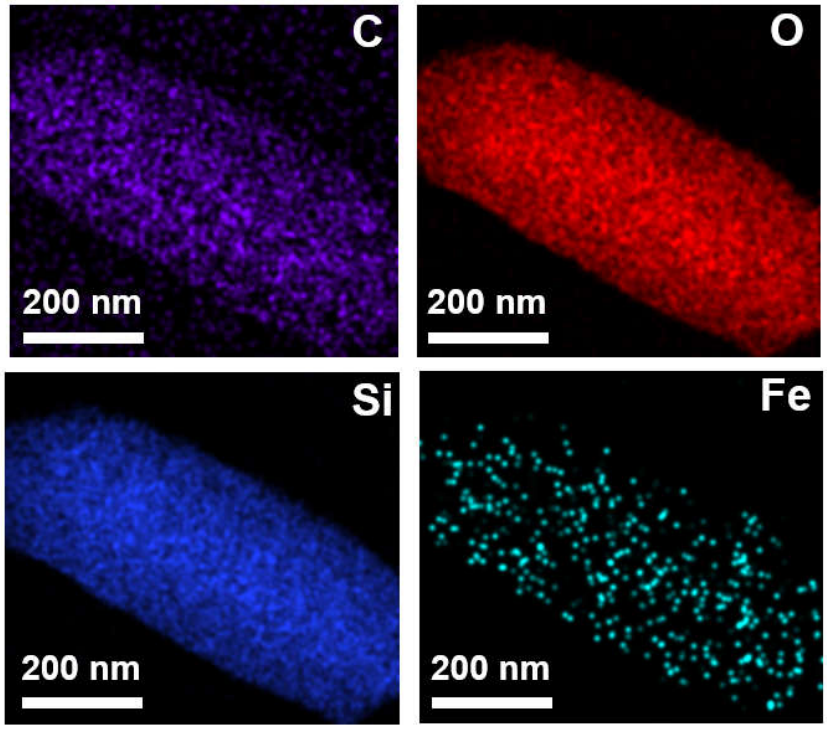

Fig. S5. STEM-EDS elemental mappings of C, O, Si and Fe of Fe_1@C-TLS.

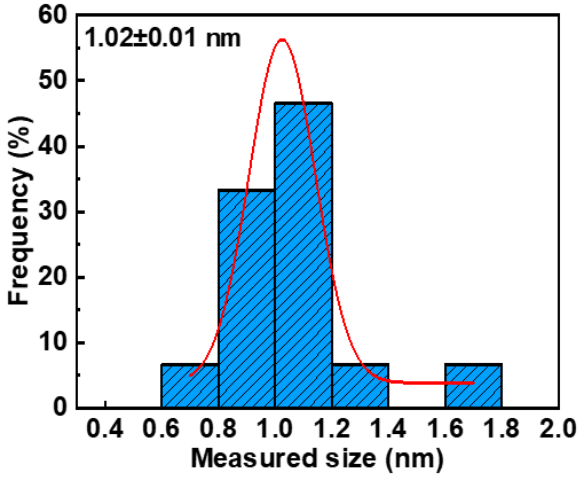

Fig. S6. Particle size distribution diagram of Fe@TRS.

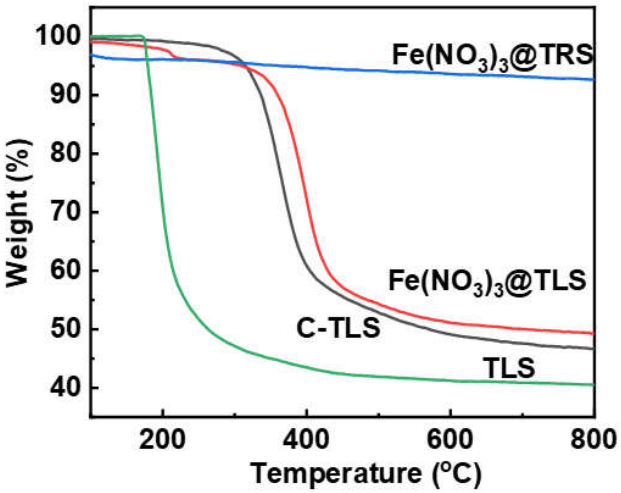

Fig. S7. TG curves of $Fe(NO_3)_3$@TLS, $Fe(NO_3)_3$@TRS, C-TLS and TLS samples.

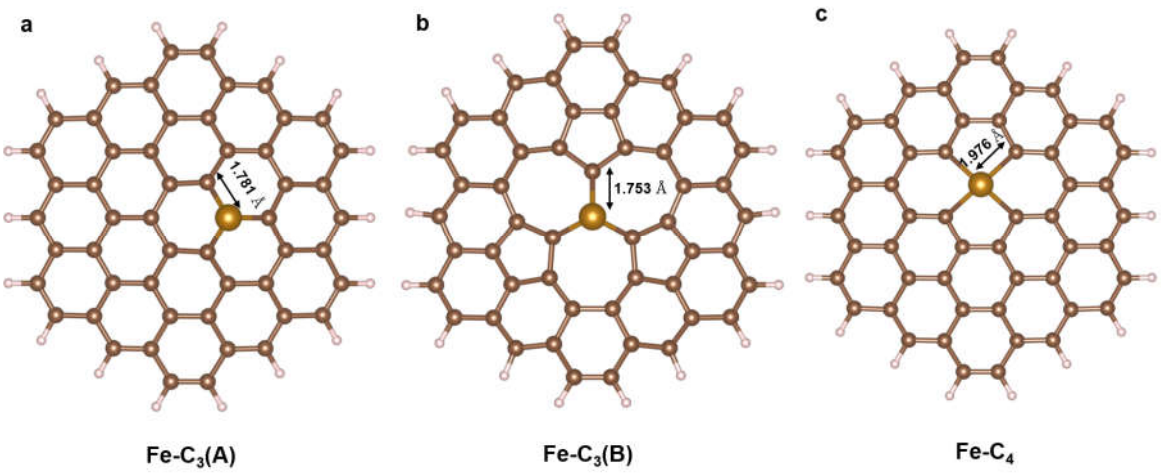

Fig. S8. Single Fe atom with (a) Fe-C_3(A), (b) Fe-C_3(B), and (c) Fe-C_4 configuration.

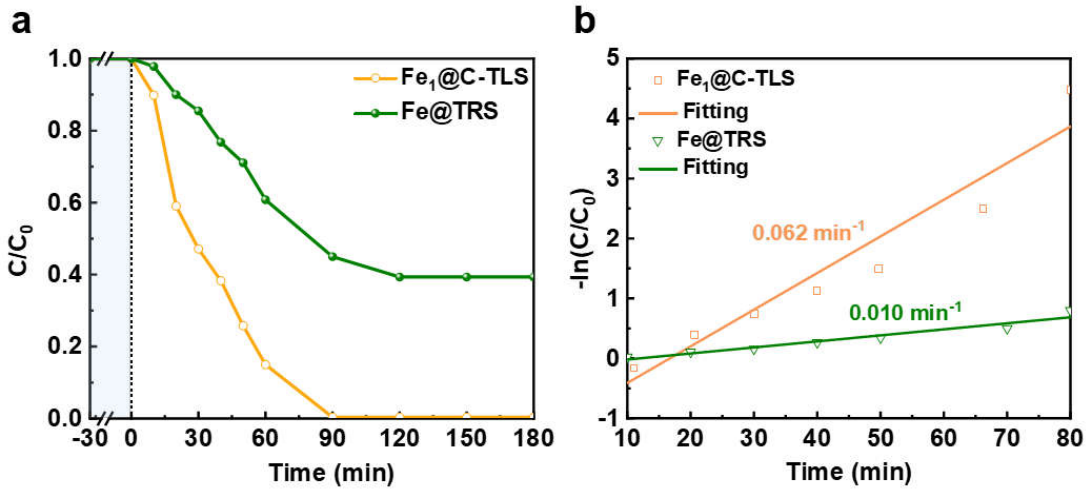

Fig. S9. (a) The degradation of phenol by Fe@TRS and Fe_1@C-TLS (reaction conditions: [pH] = 3.0 ± 0.2, [catalyst] = 0.1 g/L, [phenol] = 20 mg/L, [H_2O_2] = 1000 ppm, [T] = 30 °C). (b) The corresponding kinetic curves for phenol degradation by Fe@TRS and Fe_1@C-TLS at 30 °C.

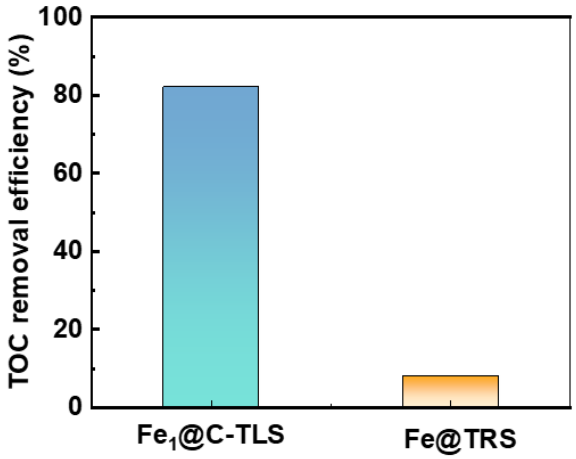

Fig. S10. The TOC removal efficiency of Fe_1@C-TLS and Fe@TRS after a 180-minute reaction.

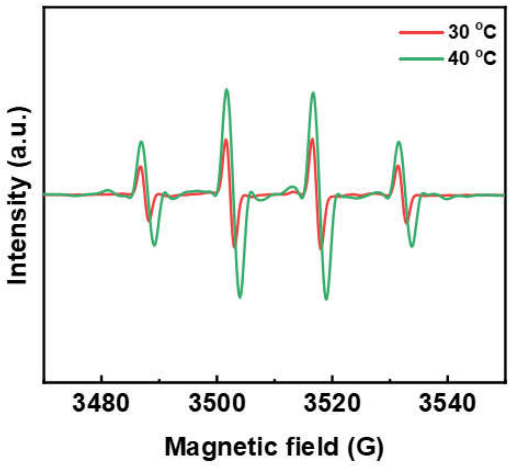

Fig. S11. EPR spectra of the Fenton reaction catalyzed by Fe_1@C-TLS at 30 °C and 40 °C.

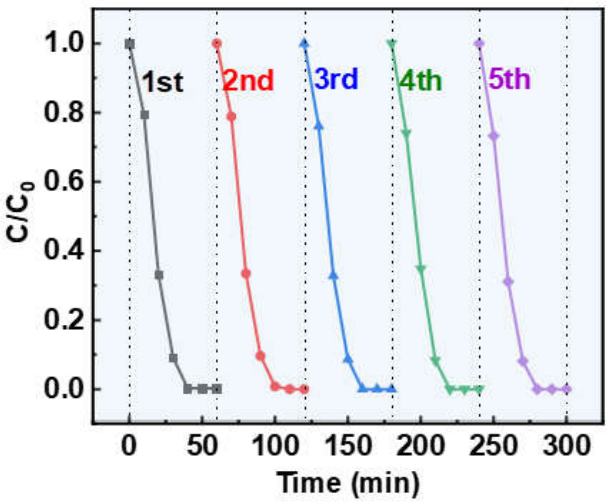

Fig. S12. Cyclic performance of Fe_1@C-TLS in the degradation of phenol.

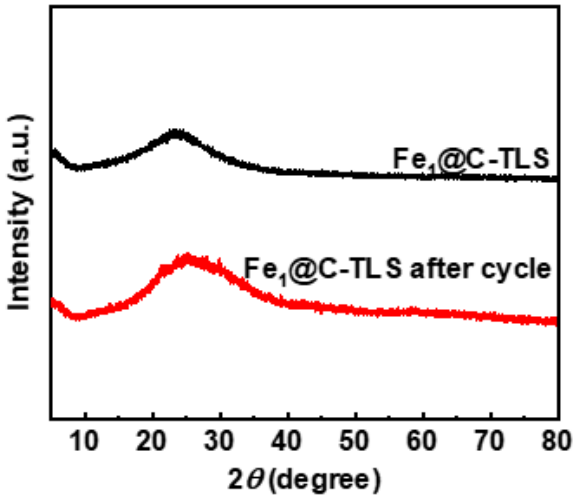

Fig. S13. XRD patterns of Fe_1@C-TLS and Fe_1@C-TLS after cycle samples.

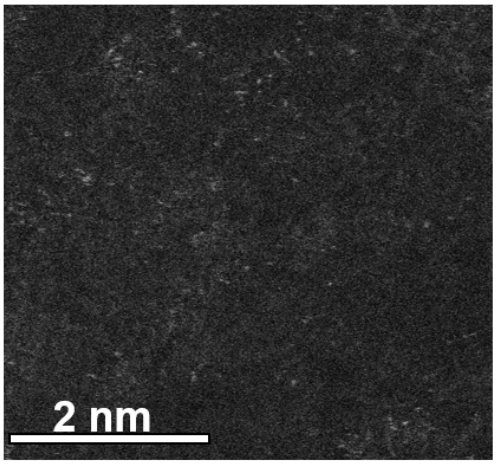

Fig. S14. HAAFD-STEM image for the sample of Fe_1@C-TLS after degradation of phenol at pH 3.

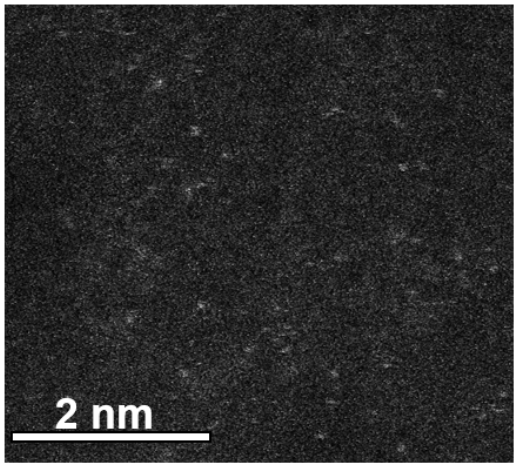

Fig. S15. HAAFD-STEM image for the sample of Fe_1@C-TLS after degradation of phenol at pH 5.

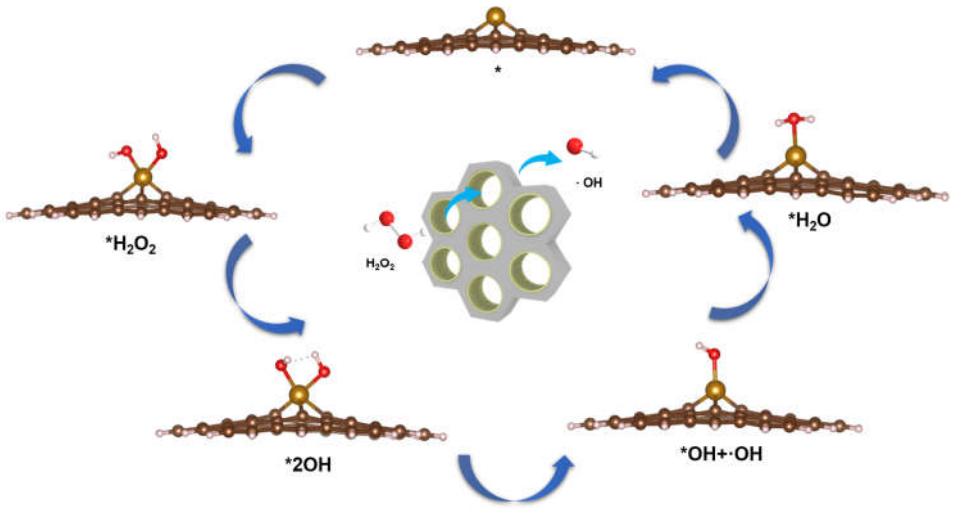

Fig. S16. Mechanism diagram of the H_2O_2 adsorption produces •OH process.

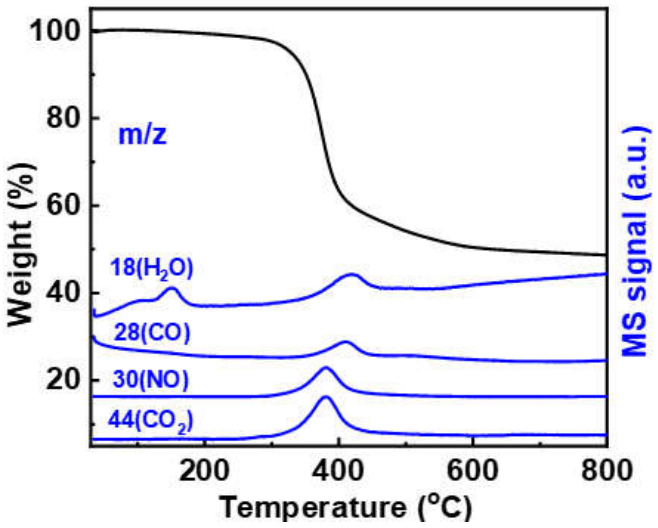

Fig. S17. TG-MS curves of C-TLS.

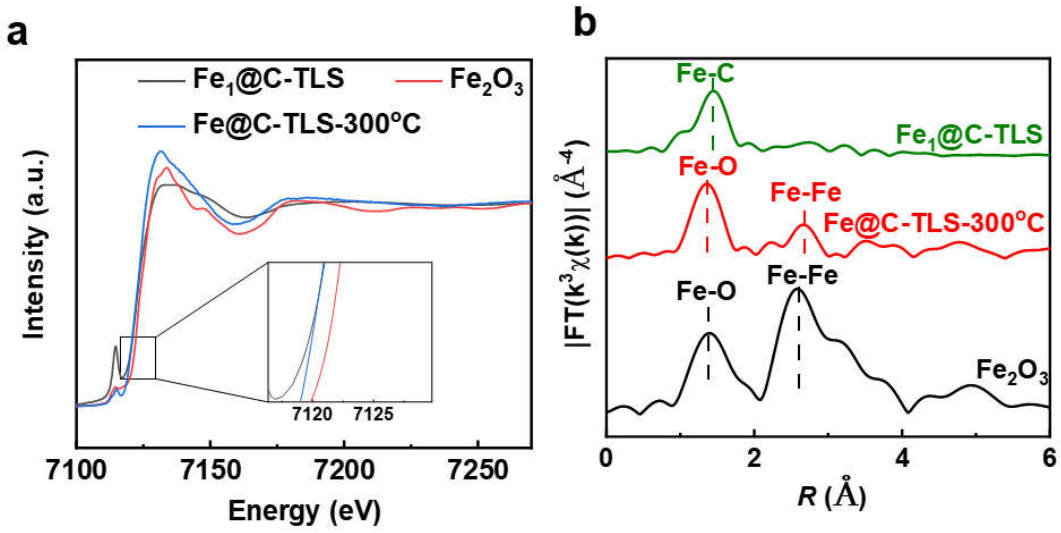

Fig. S18. (a) Normalized K-edge XANES spectra of Fe_1@C-TLS, Fe@C-TLS-300 °C, and Fe_2O_3. (b) Fourier transform k^3-weighted EXAFS spectra of Fe_1@C-TLS, Fe@C-TLS-300 °C, and Fe_2O_3. Fe@C-TLS-300 °C is the sample after heat treatment at 300 °C under argon atmosphere.

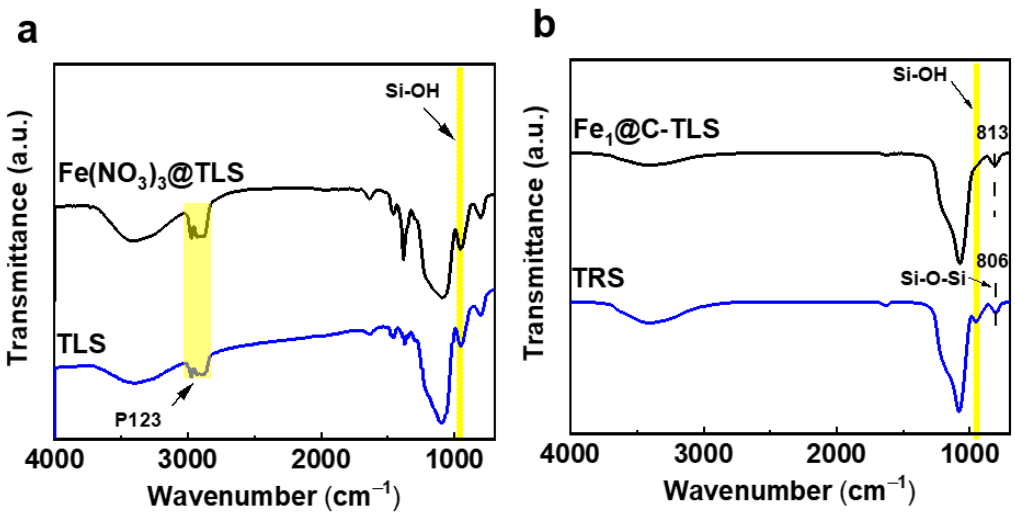

Fig. S19. IR spectra of TRS and Fe_1@C-TLS samples (a) before and (b) after heat treatment.

References

(1) Neese, F. The ORCA program system. *WIREs Comput. Mol. Sci.* **2011**, *2* (1), 73-78. DOI: 10.1002/wcms.81.

(2) Neese, F. Software Update: The ORCA Program System—Version 6.0. *WIREs Comput. Mol. Sci.* **2025**, *15* (2), e70019. DOI: 10.1002/wcms.70019.

(3) Brandenburg, J. G.; Bannwarth, C.; Hansen, A.; Grimme, S. B97-3c: A revised low-cost variant of the B97-D density functional method. *J. Chem. Phys* **2018**, *148* (6), 064104. DOI: 10.1063/1.5012601 (acccessed 9/8/2025).

(4) Grimme, S.; Antony, J.; Ehrlich, S.; Krieg, H. A consistent and accurate ab initio parametrization of density functional dispersion correction (DFT-D) for the 94 elements H-Pu. *J. Chem. Phys* **2010**, *132* (15), 154104. DOI: 10.1063/1.3382344 (acccessed 9/8/2025).

(5) Ásgeirsson, V.; Birgisson, B. O.; Bjornsson, R.; Becker, U.; Neese, F.; Riplinger, C.; Jónsson, H. Nudged Elastic Band Method for Molecular Reactions Using Energy-Weighted Springs Combined with Eigenvector Following. *J. Chem. Theory Comput.* **2021**, *17* (8), 4929-4945. DOI: 10.1021/acs.jctc.1c00462.

(6) Aleksandr V. Marenich, C. J. C., * Donald G. Truhlar*. Universal solvation model based on solute electron density and on a continuum model of the solvent defined by the bulk dielectric constant and atomic surface tension. *J. Phys. Chem. B* **2009**, *113* (18), 6378–6396. DOI: 10.1021/jp810292n.

(7) Zhu, R.; Zhu, Y.; Xian, H.; Yan, L.; Fu, H.; Zhu, G.; Xi, Y.; Zhu, J.; He, H. CNTs/ferrihydrite as a highly efficient heterogeneous Fenton catalyst for the degradation of bisphenol A: The important role of CNTs in accelerating Fe(III)/Fe(II) cycling. *Appl. Catal. B-Environ.* **2020**, *270*, 118891. DOI: 10.1016/j.apcatb.2020.118891.

(8) Zhu, Y.; Xie, Q.; Zhu, R.; Lv, Y.; Xi, Y.; Zhu, J.; Fan, J. Hydrothermal carbons/ferrihydrite heterogeneous Fenton catalysts with low H_2O_2 consumption and the effect of graphitization degrees. *Chemosphere* **2022**, *287*. DOI: 10.1016/j.chemosphere.2021.131933.

(9) Chen, F.; Wu, X. L.; Shi, C.; Lin, H.; Chen, J.; Shi, Y.; Wang, S.; Duan, X. Molecular engineering toward pyrrolic N-Rich M-N_4 (M = Cr, Mn, Fe, Co, Cu) single-atom sites for enhanced heterogeneous Fenton-Like reaction. *Adv. Funct. Mater.* **2021**, *31* (13), 2007877 DOI: 10.1002/adfm.202007877.

(10) Feng, Y.; Liao, C.; Shih, K. Copper-promoted circumneutral activation of H_2O_2 by magnetic

$CuFe_2O_4$ spinel nanoparticles: Mechanism, stoichiometric efficiency, and pathway of degrading sulfanilamide. *Chemosphere* **2016**, *154*, 573-582. DOI: 10.1016/j.chemosphere.2016.04.019.

(11) Tang, J.; Wang, J. Metal organic framework with coordinatively unsaturated sites as efficient Fenton-like catalyst for enhanced degradation of sulfamethazine. *Environ. Sci. Technol.* **2018**, *52* (9), 5367-5377. DOI: 10.1021/acs.est.8b00092.

(12) Zhang, X.; Xu, B.; Wang, S.; Li, X.; Liu, B.; Xu, Y.; Yu, P.; Sun, Y. High-density dispersion of CuNx sites for H_2O_2 activation toward enhanced Photo-Fenton performance in antibiotic contaminant degradation. *J. Hazard. Mater.* **2022**, *423*, 127039. DOI: 10.1016/j.jhazmat.2021.127039.

(13) Jiang, J.; Wang, X.; Liu, Y.; Ma, Y.; Li, T.; Lin, Y.; Xie, T.; Dong, S. Photo-Fenton degradation of emerging pollutants over Fe-POM nanoparticle/porous and ultrathin g-C_3N_4 nanosheet with rich nitrogen defect: Degradation mechanism, pathways, and products toxicity assessment. *Appl. Catal. B-Environ.* **2020**, *278*. DOI: 10.1016/j.apcatb.2020.119349.

(14) Wang, H.; Chen, T.; Chen, D.; Zou, X.; Li, M.; Huang, F.; Sun, F.; Wang, C.; Shu, D.; Liu, H. Sulfurized oolitic hematite as a heterogeneous Fenton-like catalyst for tetracycline antibiotic degradation. *Appl. Catal. B-Environ.* **2020**, *260*. DOI: 10.1016/j.apcatb.2019.118203.

(15) Su, L.; Wang, P.; Ma, X.; Wang, J.; Zhan, S. Regulating local electron density of iron single sites by introducing nitrogen vacancies for efficient photo-Fenton process. *Angew. Chem. Int. Ed.* **2021**, *60* (39), 21261-21266. DOI: 10.1002/anie.202108937.

(16) Chen, T.; Zhu, Z.; Zhang, H.; Shen, X.; Qiu, Y.; Yin, D. Enhanced removal of veterinary antibiotic florfenicol by a Cu-Based fenton-like catalyst with wide pH adaptability and high efficiency. *ACS Omega* **2019**, *4* (1), 1982-1994. DOI: 10.1021/acsomega.8b03406.

(17) He, D.; Niu, H.; He, S.; Mao, L.; Cai, Y.; Liang, Y. Strengthened Fenton degradation of phenol catalyzed by core/shell Fe–Pd@C nanocomposites derived from mechanochemically synthesized Fe-Metal organic frameworks. *Water Res.* **2019**, *162*, 151-160. DOI: 10.1016/j.watres.2019.06.058.

(18) Gao, C.; Chen, S.; Quan, X.; Yu, H.; Zhang, Y. Enhanced Fenton-like catalysis by iron-based metal organic frameworks for degradation of organic pollutants. *J. Catal.* **2017**, *356*, 125-132. DOI: 10.1016/j.jcat.2017.09.015.

(19) Yin, Y.; Shi, L.; Li, W.; Li, X.; Wu, H.; Ao, Z.; Tian, W.; Liu, S.; Wang, S.; Sun, H. Boosting Fenton-Like reactions via single atom Fe catalysis. *Environ. Sci. Technol.* **2019**, *53* (19), 11391-11400, Article. DOI: 10.1021/acs.est.9b03342.

(20) Huang, D.; Wang, W.; Rigby, K.; Wang, X.; Chen, J.; Liu, J.; Niu, J.; Stavitski, E.; Kim, J.-H. Manipulating the Second Coordination Shell of Single-Atom Fe for Enhanced Fenton Reaction. *ACS Nano* **2025**. DOI: 10.1021/acsnano.5c13343.

(21) Qu, J.; Xu, Y.; Zhang, X.; Sun, M.; Tao, Y.; Zhang, X.; Zhang, G.; Ge, C.; Zhang, Y. Ball milling-assisted preparation of N-doped biochar loaded with ferrous sulfide as persulfate activator for phenol degradation: Multiple active sites-triggered radical/non-radical mechanism. *Appl. Catal. B-Environ.* **2022**, *316*, 121639. DOI: 10.1016/j.apcatb.2022.121639.